JAMES | Journal of Advances in Modeling Earth Systems

RESEARCH ARTICLE
10.1029/2024MS004682

A Two-Dimensional Model for Eddy Saturation and Frictional Control in the Southern Ocean

J. R. Maddison[1], D. P. Marshall[2], J. Mak[3,4], and K. Maurer-Song[2]

[1]School of Mathematics and Maxwell Institute for Mathematical Sciences, The University of Edinburgh, Edinburgh, UK, [2]Department of Physics, University of Oxford, Oxford, UK, [3]Department of Ocean Science, Hong Kong University of Science and Technology, Hong Kong, Hong Kong, [4]National Oceanography Centre, Southampton, UK

Key Points:

- A simplified model of the Antarctic Circumpolar Current is presented exhibiting eddy saturation and frictional control in equilibrium
- An intrinsic oscillatory time scale is identified that can be excited by stochastic wind forcing and results in decadal variability
- The eddy energy is found to be particularly sensitive to stochastic wind forcing whereas the thermal wind transport is not

Correspondence to:
J. R. Maddison,
j.r.maddison@ed.ac.uk

Citation:
Maddison, J. R., Marshall, D. P., Mak, J., & Maurer-Song, K. (2025). A two-dimensional model for eddy saturation and frictional control in the Southern Ocean. *Journal of Advances in Modeling Earth Systems*, *17*, e2024MS004682. https://doi.org/10.1029/2024MS004682

Received 30 AUG 2024
Accepted 11 MAR 2025

Author Contributions:
Conceptualization: J. R. Maddison, D. P. Marshall
Data curation: J. R. Maddison
Formal analysis: J. R. Maddison, D. P. Marshall
Funding acquisition: D. P. Marshall
Investigation: J. R. Maddison, J. Mak, K. Maurer-Song
Methodology: J. R. Maddison, D. P. Marshall
Project administration: D. P. Marshall
Software: J. R. Maddison
Supervision: J. R. Maddison, D. P. Marshall
Writing – original draft: J. R. Maddison
Writing – review & editing: J. R. Maddison, D. P. Marshall, J. Mak, K. Maurer-Song

Abstract The reduced sensitivity of mean Southern Ocean zonal transport with respect to surface wind stress magnitude changes, known as eddy saturation, is studied in an idealized analytical model. The model is based on the assumption of a balance between surface wind stress forcing and bottom dissipation in the planetary geostrophic limit, coupled to the GEOMETRIC form of the Gent–McWilliams eddy parameterization. The assumption of a linear stratification, together with an equation for the parameterized domain integrated total eddy energy, enables the formulation of a two component dynamical system, which reduces to the non-linear oscillator of Ambaum and Novak (2014, https://doi.org/10.1002/qj.2352) in a Hamiltonian limit. The model suggests an intrinsic oscillatory time scale for the Southern Ocean, associated with a combination of mean shear erosion by eddies and eddy energy generation by the mean shear. For Southern Ocean parameters the model suggests that perturbing the system via stochastic wind forcing may lead to relatively large excursions in eddy energy.

Plain Language Summary The Southern Ocean volume transport is linked to the global stratification to the north of the Southern Ocean. It is thus of interest to understand how the Southern Ocean volume transport responds to changes in the forcing. Eddy saturation in this case refers to the weak sensitivity of the Southern Ocean volume transport to changes in wind forcing, and this phenomenon is investigated in this work within the context of an idealized but analytically and mathematically tractable model. The model mathematically formalizes the physical arguments presented in previous works, and leads to closed form expressions for model response time scales, namely an oscillation and decay time scale. Random but sustained perturbations can be included in the model, and statistics of the model response can still be derived analytically. The simple model here advances our understanding of the governing processes related to the phenomenon of eddy saturation, with possible implications for understanding the ocean's global overturning circulation.

1. Introduction

Numerical models with an explicit representation of mesoscale eddies indicate that the Southern Ocean may be eddy saturated, with a mean zonal transport which is relatively insensitive to changes in the magnitude of the mean surface wind stress (e.g., Bishop et al., 2016; Farneti et al., 2015; Hewitt et al., 2020; Munday et al., 2013). However, in models with parameterized eddies that make use of classic forms of the Gent–McWilliams parameterization (Gent & McWilliams, 1990; Gent et al., 1995), eddy saturation is often not observed. The Gent–McWilliams scheme captures the response of baroclinic eddies to a baroclinically unstable lateral density gradient, in the form of an eddy induced overturning that opposes the density gradients which are the source of the instability. However the eddy response is constrained by properties of the eddy field, and in particular by the eddy energy (Marshall et al., 2012).

Inclusion of eddy energy information in mesoscale eddy parameterizations has become increasingly widespread, finding use in constraining the parameterized momentum forcing (e.g., Bachman, 2019; Bagaeva et al., 2020; Jansen & Held, 2014; Yankovsky et al., 2024) and in variants of the Gent–McWilliams scheme (e.g., Cessi, 2008; Eden & Greatbatch, 2008; Jansen et al., 2019; Mak et al., 2018). The principal focus of the present article is on the GEOMETRIC scheme (Mak et al., 2018; Marshall et al., 2012), which makes use of an energetically constrained form of the Gent–McWilliams coefficient, with the constraint derived (and holding exactly) in the quasi-geostrophic limit (Marshall et al., 2012). The GEOMETRIC scheme is closed via the definition of a parameterized eddy energy equation. Numerical applications of the GEOMETRIC scheme in various forms have resulted

in eddy saturation in a zonally averaged planetary geostrophic channel model (Mak et al., 2017), as well as three-dimensional primitive equation models in both idealized (Mak et al., 2018) and realistic global configuration settings (Mak, Marshall, et al., 2022).

A simple two-layer analytical model for the Southern Ocean is formulated in Straub (1993), making an assumption of weak flow at depth. An increase in mean surface wind stress forcing leads to an increased Ekman transport in the upper layer, which must be counteracted by the influence of the eddies. In order for these to exist it is necessary for the flow to be baroclinically unstable, and the condition of critical flow stability implies a mean zonal transport that is independent of surface wind stress forcing magnitude.

A physical description of eddy saturation, which considers the additional element of eddy energetics, is provided in Marshall et al. (2017). The description assumes a balance between surface wind stress and bottom form stress, connected by interfacial eddy form stress. The magnitude of the eddy form stress is controlled by the eddy energy, using the GEOMETRIC energetic bound. The argument is closed with a simple parameterized integrated eddy energy budget, with eddy energy generation balanced by a linear damping of eddy energy. Combined, this description predicts that it is the eddy energy, and not the mean zonal thermal wind transport, which increases when the mean surface wind stress is increased. This description moreover predicts "frictional control," as an increase in eddy energy dissipation must be balanced by an increase in eddy energy generation, which is achieved by an increase in mean vertical velocity shear and hence mean zonal thermal wind transport. The description in Marshall et al. (2017) is related to that in Straub (1993), except that a mean zonal thermal wind transport is selected based upon consideration of eddy energetics, rather than critical flow stability.

In Ambaum and Novak (2014) a two-dimensional dynamical system for atmospheric storm tracks is described, based upon the principles of an erosion of baroclinicity due to eddy heat fluxes, and a growth in eddy heat flux due to baroclinic instability (or the reverse of each). These are precisely the physical mechanisms as in Marshall et al. (2017)—and a crucial aspect is the assumed linear scaling of eddy heat fluxes with eddy energy (in Ambaum and Novak (2014): heat fluxes scaling with the square of the eddy amplitude). The resulting system is a non-linear oscillator, whose equilibrium response exhibits the principles of eddy saturation and frictional control (Novak et al., 2018) (with the latter termed "dissipative control" in Novak et al. (2018)). A two-dimensional dynamical system for the Antarctic Slope Current has recently been discussed in Ong et al. (2024), based upon the action of eddies on a constant density slope in a two-layer model, with the GEOMETRIC energy scaling. These are the same key physical principles as in Ambaum and Novak (2014) model, and lead to the same two-dimensional dynamical system (up to the definitions of constants, and reached from Equations 6 and 7 in Ong et al. (2024) by deriving an equation for $\sqrt{APE}$). A key result from Ambaum and Novak (2014) and Ong et al. (2024) models is the prediction of an intrinsic oscillatory time scale.

A two-dimensional dynamical system for Southern Ocean mean available potential energy and eddy kinetic energy is also derived in Sinha and Abernathey (2016), and the key physical principles are again the same: erosion of a measure of the mean flow by baroclinic instability, feeding eddy energy. However the Sinha and Abernathey (2016) system includes an equation for mean available potential energy, rather than baroclinicity, and has different physical behavior.

Novak et al. (2017) note the relationship of the Ambaum and Novak (2014) model to the earlier low-dimension models for the atmosphere described in Lorenz (1984) and P. D. Thompson (1987). The P. D. Thompson (1987) model is formed as a reduced order model for a two-level quasigeostrophic model on a β-plane. A version of this model is analyzed in Kobras et al. (2022), yielding a six dimensional system where eddy saturation and frictional/dissipative control mechanisms are discussed. This is further extended in Kobras et al. (2024) in a more complicated eight dimensional model, incorporating eddy tilt effects, where partial eddy saturation behavior can be exhibited depending on the regime.

The appearance of the same dynamical equations, emerging based on the same physical principles, motivates a more detailed study of the consequences of these principles for the dynamics of the Antarctic Circumpolar Current. In this article we return to a model of the Antarctic Circumpolar Current as in Marshall et al. (2017), and consider a simple dynamical extension. The model is specifically derived using a reduced order density equation with a single dynamical degree of freedom setting the meridional mean density gradient, combined with a version of the GEOMETRIC eddy energy budget. The model as derived here is not dissimilar to the zonally averaged planetary geostrophic channel model in Mak et al. (2017), but is constructed using the further simplifications of a

fixed linear stratification, and a time varying linear lateral density gradient (cf. A. F. Thompson et al., 2016). Specifically the mean thermal wind transport equation is arrived at using a Galerkin discretization with a single spatial degree of freedom which sets the lateral mean density gradient. Since the model derived here uses the physical principles of Ambaum and Novak (2014), the same dynamical system is once again reached (up to the definitions of constants). As a result we here obtain a simple two-dimensional model for the Antarctic Circumpolar Current which exhibits eddy saturation and frictional control in its equilibrium response, and which also predicts an intrinsic oscillatory time scale when perturbed from equilibrium.

Sensitivities to more rapid fluctuations on top of the mean surface wind stress may also be important. Eddy saturation and frictional control relate to the baroclinic processes, which operate on time scales longer than barotropic responses that are known to operate in the Southern Ocean (e.g., Hughes et al., 1999; Olbers & Lettmann, 2007; Sura & Gille, 2003). The faster time responses are usually attributed to the short term sub-annual fluctuations in the surface wind forcing over the Southern Ocean, and sometimes modeled as stochastic (e.g., Sura & Gille, 2003). It is of interest to investigate how the transport and eddy energy responds to more rapid fluctuations, and whether such fluctuations have consequences for the eddy saturation and frictional control phenomena. This is investigated in this article by considering a simple stochastic extension to the two-dimensional dynamical system, and it is found that while the mean thermal wind transport is relatively less sensitive to the stochastic forcing, the eddy energy exhibits more significant excursions away from equilibrium.

The key novel contribution of this article is the derivation of a form of the Ambaum and Novak (2014) model as applied to the Antarctic Circumpolar Current, allowing for specific predictions regarding its dynamical response, and leading to a new prediction for an intrinsic oscillatory timescale. Moreover, the use of a Galerkin discretization to derive this model provides a natural route to less idealized versions. The stochastic extension leads to further predictions, and in particular the model suggests significant Southern Ocean eddy energy response. The eddy energy response is not due to direct forcing of the turbulence, but is instead due to the system's dynamical response when perturbed from equilibrium.

The article proceeds as follows. In Section 2 the scalings of the Marshall et al. (2017) description are summarized. In Section 3 this is extended via the formulation of a two component dynamical system, which has a Hamiltonian limit governed by the non-linear oscillator dynamics of Ambaum and Novak (2014) and whose fixed point exhibits the scalings of Marshall et al. (2017) model in this limit. The response of this system to varying wind forcing is considered in Section 4, considering first the basic case of the linear response to oscillatory wind forcing, before considering the response to stochastic wind forcing. The paper concludes in Section 5.

2. Key Scalings

We start by briefly outlining the principles as described in Marshall et al. (2017). The discussion in Marshall et al. (2017) is phrased in terms of vertical momentum eddy stress. Here, and consistent with the formulation to follow, we instead outline an equivalent viewpoint in terms of Eulerian mean and eddy-induced overturning. We initially construct a basic scaling argument, and the scalings are justified more robustly, with dimensional factors restored, in Section 3.

A zonally periodic channel is considered, subject to a surface wind stress forcing with magnitude τ. The mean zonal flow has magnitude U near the surface and, as per the argument in Straub (1993), is assumed to be weak at depth.

Considering first the mean momentum balance the vertical shear leads, through thermal wind balance, to an Eulerian mean overturning, suggesting

$$\text{Eulerian mean overturning} \sim \tau. \tag{1}$$

This Eulerian mean overturning is countered by an eddy-induced overturning associated with the baroclinically unstable vertical shear. If the (total) eddy energy is E then, consistent with the GEOMETRIC scheme, this suggests the linear scaling

$$\text{Eddy-induced overturning} \sim E. \tag{2}$$

Mean momentum balance therefore suggests

$$E \sim \tau, \tag{3}$$

that is, that the eddy energy increases with increasing surface wind stress magnitude.

Now, considering the eddy energy balance, baroclinic instability leads to generation of eddy energy

$$\text{Eddy energy generation} \sim \text{Vertical shear} \times \text{Eddy energy} \sim UE. \tag{4}$$

which uses a GEOMETRIC form for the eddy form stress (Marshall et al., 2012, 2017). Assuming that eddy energy is dissipated linearly at a rate λ, that is,

$$\text{Eddy energy dissipation} \sim \lambda E, \tag{5}$$

eddy energy balance therefore suggests

$$U \sim \lambda. \tag{6}$$

This is the "frictional control" mechanism described in Marshall et al. (2017), with the mean flow magnitude increasing with increasing dissipation. Since U is independent of τ, these arguments imply eddy saturation.

These arguments, which follow Marshall et al. (2017), imply that the momentum input τ sets the scale of the total eddy energy E, and the magnitude of eddy energy dissipation λ sets the mean zonal momentum.

3. Dynamical Equations

3.1. Density Profile

We now consider a zonally periodic channel $(x, y, z) \in [0, L_x] \times [-L/2, L/2] \times [-H, 0]$, with a linearly varying mean density profile defined (up to the addition of a constant) to be

$$\rho(y, z, t) = -\frac{\rho_0}{g} m(t) y - \frac{\rho_0}{g} N^2 z. \tag{7}$$

Here ρ_0 is a constant reference density, g the magnitude of the gravitational acceleration, and N the buoyancy frequency, all assumed to be constant. A time-dependent function $m(t)$ sets the horizontal density gradient. The domain integrated density is constant for all $m(t)$, which ensures conservation of the integrated density in the reduced order model to follow. The zonal, meridional, and vertical coordinates are denoted x, y, and z respectively, and t is time. Defining a (non-perturbation) buoyancy $b = -g\rho/\rho_0$ we have

$$b(y, z, t) = m(t) y + N^2 z. \tag{8}$$

Thermal wind balance on an f-plane leads to a mean thermal wind transport

$$T(t) = -\frac{1}{2} L H^2 \frac{1}{f} m(t), \tag{9}$$

where f is the Coriolis parameter. Hence the mean buoyancy may be written

$$b(y, z, t) = -2 \frac{1}{L H^2} f T(t) y + N^2 z. \tag{10}$$

3.2. Mean Thermal Wind Transport

We now construct a model subject to near surface wind forcing, balancing near base momentum dissipation, with eddies represented by a form of the Gent–McWilliams parameterization. In this model the mean buoyancy is

subject to a near surface wind driven Ekman transport, which is closed by near boundary transports around the edges of the domain. Through thermal wind balance this generates a mean vertically sheared flow, and baroclinic eddies which feed on this shear should then oppose the mechanism that generated them. The eddies should therefore also lead to a near boundary eddy induced transport that opposes the transport set up by the wind. We restrict to a single spatial degree of freedom for the density by asserting that the density varies linearly in space, and by asserting that the buoyancy frequency is fixed. A Galerkin discretization allows us to construct an equation involving the single remaining spatial degree of freedom, and the result is a time-dependent equation for the mean thermal wind transport.

We start from a mean buoyancy equation in the form

$$\frac{\partial b}{\partial t} + \frac{\partial}{\partial y}[(v + v^*)\, b] + \frac{\partial}{\partial z}[(w + w^*)\, b] = 0, \tag{11}$$

where v and w are the meridional and vertical components of the mean velocity, and v^* and w^* are corresponding components of an eddy-induced transport velocity. The Galerkin discretization uses the mean buoyancy Equation 11, with a discrete mean buoyancy having a single spatial degree of freedom setting the lateral mean buoyancy gradient as per Equation 10.

Multiplying by y and integrating leads to

$$\frac{\mathrm{d}}{\mathrm{d}t}\int_{-L/2}^{L/2}\int_{-H}^{0} by \,\mathrm{d}z\,\mathrm{d}y = \int_{-L/2}^{L/2}\int_{-H}^{0} (v + v^*)\, b \,\mathrm{d}z\,\mathrm{d}y, \tag{12}$$

where no-normal-flow boundary conditions are assumed. For the mean buoyancy profile (Equation 10) we have

$$\frac{\mathrm{d}}{\mathrm{d}t}\int_{-L/2}^{L/2}\int_{-H}^{0} by \,\mathrm{d}z\,\mathrm{d}y = -\frac{1}{6}\frac{L^2}{H} f \frac{\mathrm{d}T}{\mathrm{d}t}. \tag{13}$$

From the planetary geostrophic mean zonal momentum equation we have

$$-fv = F - D, \tag{14}$$

where F and D represent mean zonal momentum forcing and dissipation respectively. Assuming that the system is forced by a wind stress concentrated to a near surface region, balanced by a bottom stress of equal and opposite magnitude concentrated to a near base region, leads to

$$-\int_{-L/2}^{L/2}\int_{-H}^{0} fvb \,\mathrm{d}z\,\mathrm{d}y = \frac{\tau}{\rho_0}\int_{-L/2}^{L/2}\int_{-H}^{0} [\delta(z) - \delta(z + H)]\, b \,\mathrm{d}z\,\mathrm{d}y, \tag{15}$$

where τ defines the surface wind stress and where $\delta(\cdot)$ denotes the Dirac delta. Consistent with the idealized model in Mak et al. (2017) we here apply a local balance between surface wind stress and bottom stress. For the mean buoyancy profile (Equation 10) this gives

$$\int_{-L/2}^{L/2}\int_{-H}^{0} vb \,\mathrm{d}z\,\mathrm{d}y = -LH\frac{N^2}{f}\frac{\tau}{\rho_0}. \tag{16}$$

Writing the eddy-induced transport velocity in terms of the eddy transport stream function

$$v^* = \frac{\partial \psi}{\partial z} \tag{17}$$

leads to

$$\int_{-L/2}^{L/2}\int_{-H}^{0} v^{*}b\,\mathrm{d}z\,\mathrm{d}y = \int_{-L/2}^{L/2}\int_{-H}^{0}\frac{\partial\psi}{\partial z}b\,\mathrm{d}z\,\mathrm{d}y = -\int_{-L/2}^{L/2}\int_{-H}^{0}\psi\frac{\partial b}{\partial z}\,\mathrm{d}z\,\mathrm{d}y, \tag{18}$$

where $\psi = 0$ on boundaries has been used. Applying the Gent–McWilliams parameterization (Gent & McWilliams, 1990; Gent et al., 1995) we have, in the interior

$$\psi = \kappa_{\mathrm{GM}}\frac{\partial b}{\partial y}\left(\frac{\partial b}{\partial z}\right)^{-1}, \tag{19}$$

and $\psi = 0$ on boundaries. That is, κ_{GM} is defined to be spatially constant within the interior, and then falls rapidly to zero near the boundaries. For the mean buoyancy profile (Equation 10), we obtain

$$\int_{-L/2}^{L/2}\int_{-H}^{0} v^{*}b\,\mathrm{d}z\,\mathrm{d}y = 2\frac{1}{H}f\kappa_{\mathrm{GM}}T. \tag{20}$$

Combining Equations 12, 13, 16, and 20 then leads to an equation for the mean thermal wind transport

$$\frac{\mathrm{d}T}{\mathrm{d}t} = 6\frac{H^2}{L}\frac{N^2}{f^2}\frac{\tau}{\rho_0} - 12\frac{1}{L^2}\kappa_{\mathrm{GM}}T. \tag{21}$$

The two right-hand-side terms correspond to the competition between generation of mean thermal wind transport due to the wind-driven Eulerian overturning (first term), and erosion by baroclinic instability (second term). Alternatively this may be interpreted in terms of a balance between near surface wind and eddy stress,

$$\frac{\mathrm{d}T}{\mathrm{d}t} = 6\frac{H^2}{L}\frac{N^2}{f^2}\frac{1}{\rho_0}\left[\tau - 2\rho_0\frac{1}{LH^2}\frac{f^2}{N^2}\kappa_{\mathrm{GM}}T\right], \tag{22}$$

where the second bracketed term is the vertical eddy stress.

The mean thermal wind transport equation arrived at is similar to the Southern Ocean component of the Gnanadesikan (1999)-type model described in Allison et al. (2011). In Allison et al. (2011) the evolution of a single isopycnal is modeled, and the channel is coupled to an inter-hemispheric basin. Here instead the model uses a continuous linear stratification in a bounded channel. Moreover Allison et al. (2011) uses a fixed and constant value for the Gent–McWilliams coefficient.

3.3. GEOMETRIC and Eddy Energetics

Eddy saturation is possible at the steady state of Equation 21 if the magnitude of the Gent–McWilliams coefficient κ_{GM} scales with the magnitude of the surface wind stress τ. From Equation 22 we have, at steady-state, the mean stress balance

$$\tau = 2\rho_0\frac{1}{LH^2}\frac{f^2}{N^2}\kappa_{\mathrm{GM}}T. \tag{23}$$

The key piece of extra physics added by the GEOMETRIC closure is to achieve a scaling of κ_{GM} with surface wind stress *indirectly*, by allowing the Gent–McWilliams coefficient to scale with eddy energy (see Mak et al., 2017). An important and easily overlooked aspect of the GEOMETRIC form of κ_{GM} is that it also scales inversely with the lateral mean density gradient. In this idealized model this means that $\kappa_{\mathrm{GM}}T$ scales with eddy energy E, but is independent of mean thermal wind transport T. At steady state the mean stress balance then sets the eddy energy, but does not set the mean thermal wind transport. Instead the mean thermal wind transport at steady state is set by a balance between eddy energy production and eddy energy dissipation.

For the mean buoyancy profile (Equation 8) GEOMETRIC defines a Gent–McWilliams coefficient (Marshall et al., 2012)

$$\kappa_{\mathrm{GM}} = \alpha E \frac{N}{|m|}, \tag{24}$$

where α is a non-dimensional constant which in the quasi-geostrophic limit has a maximum magnitude of one (Marshall et al., 2012), and is here assumed to be positive, consistent with baroclinic instability of the mean flow. E is the eddy energy per unit mass, so that the domain integrated total eddy energy is

$$\mathcal{E} = L_x \int_{-L/2}^{L/2} \int_{-H}^{0} \rho_0 E \, \mathrm{d}z \, \mathrm{d}y. \tag{25}$$

Assuming that both κ_{GM} and α are spatially constant (in the interior) and using (Equation 9) yields (for fT negative, and in the interior)

$$\kappa_{\mathrm{GM}} = -\frac{1}{2}\alpha L H^2 \frac{N}{f}\frac{E}{T}. \tag{26}$$

Hereafter we refer to the energy per unit mass as simply an "energy."

GEOMETRIC includes an equation for a depth-integrated parameterized total eddy energy budget. Here this is further simplified by considering a fully domain integrated budget (see Mak et al., 2017),

$$\frac{\mathrm{d}E}{\mathrm{d}t} = \frac{1}{LH}\int_{-L/2}^{L/2}\int_{-H}^{0} \kappa_{\mathrm{GM}} \left(\frac{\partial b}{\partial y}\right)^2 \left(\frac{\partial b}{\partial z}\right)^{-1} \mathrm{d}z \, \mathrm{d}y - \lambda E + \lambda E_0. \tag{27}$$

The first right-hand-side term represents the mean-to-eddy energy conversion, the second a linear damping of eddy energy, and the third a background source of eddy energy. λ defines a linear damping rate for the eddy energy per unit mass toward E_0. E_0, included in the parameterized eddy energy budget in Mak, Marshall, et al. (2022), damps the eddy energy toward a background level, but might also be a very basic representation of any other sources of eddy energy generation.

The assumption of linear damping is a highly simplified approximation for eddy energy dissipation. A simple assumption of linear damping is used principally for consistency with Mak et al. (2017) and Marshall et al. (2017), but also because of the resulting analytic tractability, and because of the absence of a clearly better alternative. Appendix A considers a slightly more general case of non-linear eddy energy dissipation.

3.4. Two-Dimensional Dynamical System

Using the GEOMETRIC form of the Gent–McWilliams coefficient (Equation 26) with spatially constant κ_{GM} and α (in the interior), for the case where the product fT is negative and for the mean buoyancy profile (Equation 10), Equations 21 and 27 become

$$\frac{\mathrm{d}T}{\mathrm{d}t} = 6\frac{H^2}{L}\frac{N^2}{f^2}\left[\frac{\tau}{\rho_0} + \alpha\frac{f}{N}E\right], \tag{28a}$$

$$\frac{\mathrm{d}E}{\mathrm{d}t} = \left[-2\alpha\frac{1}{LH^2}\frac{f}{N}T - \lambda\right]E + \lambda E_0, \tag{28b}$$

yielding a two-dimensional system of ordinary differential equations for the mean thermal wind transport and total eddy energy.

If these equations are generalized to include positive fT (noting that this requires $|m| \rightarrow -|m|$ in Equation 24) then this permits mean thermal wind transport reversal with baroclinic stability. This unphysical case is included as it is technically needed later, for example, when stochastic forcing is added.

Table 1
Southern Ocean Relevant Parameters

Parameter	Symbol	Value
Wind stress	τ	0.1 N m^{-2}
Buoyancy frequency	N	$-30f$
Density	ρ_0	10^3 kg m^{-3}
Meridional domain size	L	2,000 km
Depth	H	3 km
GEOMETRIC eddy efficiency parameter	α	0.1
Eddy energy dissipation rate	λ	10^{-7} s^{-1}

Note. See for example, Mak, Avdis, et al. (2022) for eddy energy dissipation rate estimates. These define a non-dimensional squared angular frequency $\tilde{\omega}_0^2 = 0.09$, and correspond to an oscillatory time scale of $\sim 2\pi/(\tilde{\omega}_0\lambda) = 6.6$ years.

3.5. Steady State, Eddy Saturation, and Frictional Control

We can now see the balances inherent in the model of Marshall et al. (2017). The bracketed term in the mean momentum Equation 28a involves the eddy energy, and the bracketed term in the eddy energy Equation 28b involves the mean momentum. At steady-state (for small E_0) we find that the mean momentum balance sets the eddy energy, and the eddy energy balance sets the mean momentum.

Specifically, at steady state (i.e., at the fixed point) we obtain mean thermal wind transport and eddy energy

$$T_* = -\frac{1}{2}\frac{1}{\alpha}LH^2\frac{N}{f}\lambda\left[1 - \frac{E_0}{E_*}\right], \tag{29a}$$

$$E_* = -\frac{1}{\alpha}\frac{N}{f}\frac{\tau}{\rho_0}. \tag{29b}$$

Note that with small background energy generation E_0, the mean thermal wind transport is independent of wind stress τ, and scales with the eddy energy dissipation λ, while the eddy energy scales with the wind stress τ. These are eddy saturation and frictional control, being set by mechanisms consistent with those described in Marshall et al. (2017).

With $E_0 = 0$ the Southern Ocean relevant parameters as in Table 1 lead to a steady state thermal wind transport of $T_* = 270$ Sv and a steady state Gent-McWilliams coefficient of 3,000 m^{2}s^{-1}. While the precise value for the transport is somewhat too high these have a reasonable order of magnitude.

3.6. Non-Dimensionalization

It is natural to use the steady state to define a non-dimensionalization, with non-dimensional mean thermal wind transport $\tilde{T}$ and eddy energy $\tilde{E}$ defined

$$T = \hat{T}\tilde{T}, \tag{30a}$$

$$E = \hat{E}\tilde{E}, \tag{30b}$$

with

$$\hat{T} = -\frac{1}{2}\frac{1}{\alpha}LH^2\frac{N}{f}\lambda, \tag{31a}$$

$$\hat{E} = E_* = -\frac{1}{\alpha}\frac{N}{f}\frac{\tau}{\rho_0}. \tag{31b}$$

A non-dimensional background energy is defined similarly, $\tilde{E}_0 = E_0/\hat{E}$. The eddy energy dissipation parameter λ defines an inverse time scale, leading to a non-dimensionalized time $\tilde{t} = \lambda t$. Considering the logarithm of the non-dimensionalized eddy energy $\tilde{M} = \ln\tilde{E}$, then leads to

$$\frac{d\tilde{T}}{d\tilde{t}} = -\tilde{\omega}_0^2\left(e^{\tilde{M}} - 1\right), \tag{32a}$$

$$\frac{d\tilde{M}}{d\tilde{t}} = \left(\tilde{T} - 1\right) + \tilde{E}_0 e^{-\tilde{M}}, \tag{32b}$$

where a non-dimensional squared angular frequency is defined

$$\tilde{\omega}_0^2 = -12\alpha \frac{1}{L^2}\frac{N}{f}\frac{\tau}{\rho_0}\frac{1}{\lambda^2}. \tag{33}$$

For $E_0 = 0$ the Ambaum and Novak (2014) model is now obtained.

3.7. Hamiltonian Structure

Considering $\tilde{E}_0 = 0$ leads to

$$\frac{\mathrm{d}\tilde{T}}{\mathrm{d}\tilde{t}} = -\tilde{\omega}_0^2\left(e^{\tilde{M}} - 1\right), \tag{34a}$$

$$\frac{\mathrm{d}\tilde{M}}{\mathrm{d}\tilde{t}} = \left(\tilde{T} - 1\right). \tag{34b}$$

These correspond directly to Equation 6 in Ambaum and Novak (2014), and Equations 6 and 7 in Ong et al. (2024) (in the latter after deriving an equation for $\sqrt{APE}$). By analogy with a standard linear oscillator, $\mathrm{d}^2u/\mathrm{d}t^2 = -ku$ with "stiffness" parameter k, we can here define a non-linear and non-dimensional stiffness parameter

$$\tilde{k} = \tilde{\omega}_0^2\left(\frac{e^{\tilde{M}} - 1}{\tilde{M}}\right) = \tilde{\omega}_0^2\left(\frac{\tilde{E} - 1}{\ln\tilde{E}}\right), \tag{35}$$

which indicates that the eddy energy is more rapidly restored to equilibrium at large energy. Correspondingly, away from equilibrium the system spends longer periods at weak eddy energies with mean thermal wind transport growing due to Eulerian mean overturning, interspersed with relatively shorter bursts of higher eddy energy with mean thermal wind transport falling via baroclinic instability.

Defining a Hamiltonian (equivalent up to scaling to Equation 9 of Ambaum and Novak (2014))

$$\mathcal{H}\left(\tilde{T},\tilde{M}\right) = \frac{1}{2}\left(\tilde{T} - 1\right)^2 + \tilde{\omega}_0^2\left(e^{\tilde{M}} - 1 - \tilde{M}\right), \tag{36}$$

Equation 34 are equivalent to

$$\frac{\mathrm{d}\tilde{T}}{\mathrm{d}\tilde{t}} = -\frac{\partial\mathcal{H}}{\partial\tilde{M}}, \tag{37a}$$

$$\frac{\mathrm{d}\tilde{M}}{\mathrm{d}\tilde{t}} = +\frac{\partial\mathcal{H}}{\partial\tilde{T}}. \tag{37b}$$

Here the Hamiltonian is defined such that it is non-negative and vanishes only at the fixed point. With this convention the mean thermal wind transport is the conjugate momentum.

Away from equilibrium the system orbits on contours of the Hamiltonian—see Figure 1. These orbits correspond to the mechanism shown schematically in Figure 2, with the same fundamental principles appearing in Figure 10 of Ong et al. (2024) in their model for the Antarctic Slope Current. Starting from low eddy energies and low mean thermal wind transport, the Eulerian mean overturning due to the wind stress is only weakly opposed, leading to a growth in the mean thermal windshear (lower part of the orbit in Figure 1). A sufficiently high shear drives an increase in the eddy energy via baroclinic instability (right part of the orbit) which, once the eddy energy is sufficiently high, counteracts the mean overturning and erodes the mean thermal windshear (upper part of the orbit). A sufficiently weakened mean thermal windshear, with correspondingly weakened eddy energy generation, is no longer able to support the eddy energy against dissipation, and so the eddy energy decays (left part of the orbit). The mechanism behind the oscillatory eddy energy response is reminiscent of the overshoot behavior

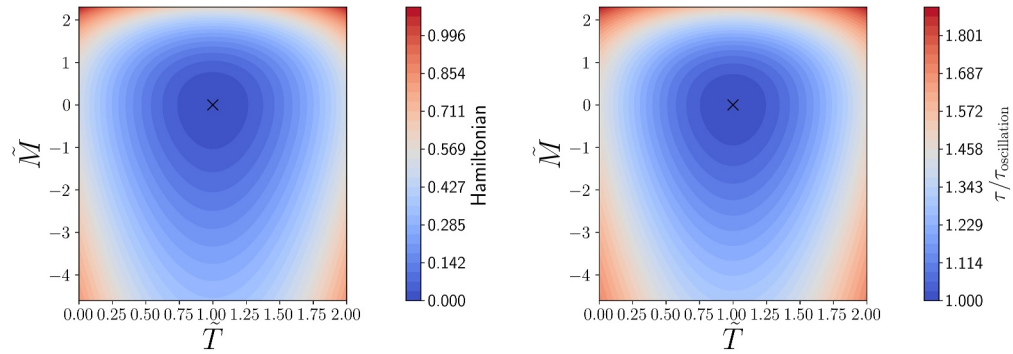

Figure 1. Left: Hamiltonian (Equation 36) for Southern Ocean relevant parameters as in Table 1, corresponding to $\tilde{\omega}_0^2 = 0.09$. The dynamics orbits on contours in an anti-clockwise sense. Right: Orbit time scales, computed using action-angle coordinators. The crosses indicate the fixed point.

behind the oscillatory finite amplitude response in the inviscid cases of the two-layer model for baroclinic instability in Pedlosky (1970), and also of the "charge and discharge" regime described in Kobras et al. (2024).

Differentiating the maximum non-dimensional mean thermal wind transport and eddy energy with respect to the Hamiltonian leads to

$$\frac{\mathrm{d}\tilde{T}_{\max}}{\mathrm{d}\mathcal{H}} = \frac{1}{\tilde{T}_{\max} - 1}, \tag{38a}$$

$$\frac{\mathrm{d}\tilde{E}_{\max}}{\mathrm{d}\mathcal{H}} = \frac{1}{\tilde{\omega}_0^2} \frac{\tilde{E}_{\max}}{\tilde{E}_{\max} - 1}. \tag{38b}$$

Note the extra factor of $1/\tilde{\omega}_0^2$ which appears in the latter expression, for the eddy energy, but not in the former, for the mean thermal wind transport. For Southern Ocean relevant parameters listed in Table 1, the parameter $\tilde{\omega}_0^2 = 0.09$ is relatively small, amplifying the effect on the eddy energetics when perturbed from the equilibrium. That is, perturbed dynamics can exhibit excursions to relatively large eddy energy.

4. Response to Forcing

4.1. Time Scales

At the fixed point (Equation 29) the Jacobian of the system (Equation 28) has eigenvalues

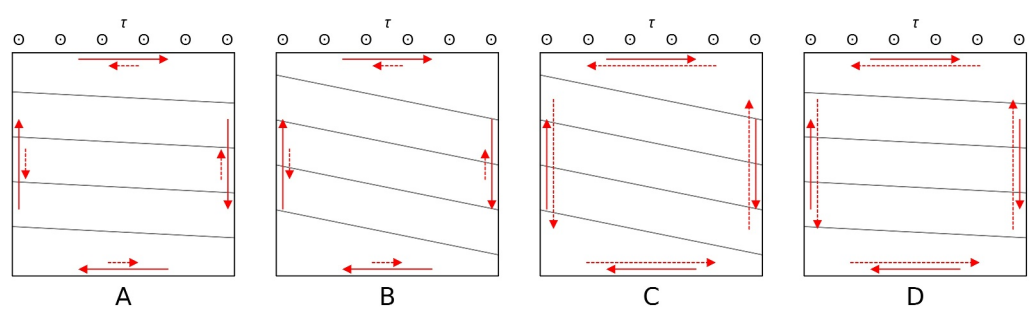

Figure 2. The mechanism of the non-linear oscillation. Density surfaces are indicated in gray, the Eulerian overturning circulation with solid arrows, and the eddy induced circulation with dashed arrows. A to B: The surface wind stress drives an Eulerian overturning, increasing lateral mean density gradients and hence the mean thermal wind transport. B to C: The increased mean thermal windshear leads to a growth in eddy energy via baroclinic instability. C to D: The eddy induced overturning overcomes the Eulerian overturning, eroding the lateral mean density gradients and hence the mean thermal wind transport. D to A: As the mean thermal windshear erodes, baroclinic instability weakens, and eddy energy decays. The same fundamental principles appear in Figure 10 of Ong et al. (2024) in a model for the Antarctic Slope Current.

$$\Lambda_{\pm} = -\frac{1}{\tau_{\text{decay}}} \pm i\frac{2\pi}{\tau_{\text{oscillation}}}, \tag{39}$$

with

$$\tau_{\text{decay}} = 2\frac{E_*}{E_0}\frac{1}{\lambda}, \tag{40a}$$

$$\tau_{\text{oscillation}} = \frac{2\pi}{\sqrt{\omega_0^2 - \frac{1}{\tau_{\text{decay}}^2}}}, \tag{40b}$$

where $\omega_0 = \tilde{\omega}_0\lambda$. Perturbing the system from the fixed point, in the linearized case and for $\tau_{\text{oscillation}}$ real, leads to the mean thermal wind transport and logarithm eddy energy each oscillating with period $\tau_{\text{oscillation}}$. The amplitudes of the oscillations decay exponentially with decay rate $1/\tau_{\text{decay}}$.

Assuming τ_{decay} is sufficiently long so that $\tau_{\text{oscillation}}$ is real, if $E_0 > 0$ then the fixed point is a stable focus with trajectories spiraling anti-clockwise in $\left(\tilde{T}, \tilde{M}\right)$ phase space toward the fixed point (Equation 29) with linearized decay time scale τ_{decay}. Here $E_0 > 0$ breaks the Hamiltonian structure, leading to a decay toward the fixed point. A stronger eddy energy dissipation can also be used as alternative mechanism for breaking the Hamiltonian structure—see Appendix A.

Since the equilibrium eddy energy E_* scales linearly with the wind stress magnitude, for $E_0 > 0$ the decay time scale also scales linearly with the wind stress magnitude.

For a long decay time scale there is a linearized oscillatory time scale

$$\tau_{\text{oscillation}} = \frac{2\pi}{\omega_0} = \frac{\pi}{\sqrt{3}}\sqrt{-\frac{1}{\alpha}L^2\frac{f}{N}\frac{\rho_0}{\tau}}, \tag{41}$$

which is $1/\sqrt{2\alpha}$ times the oscillatory time scale in Ong et al. (2024). To see the mechanisms setting the angular frequency ω_0, and hence the time scale $\tau_{\text{oscillation}}$, note that the dynamical system (Equation 28) can be re-written, for $E_0 = 0$,

$$\frac{\mathrm{d}S}{\mathrm{d}t} = 12\frac{1}{L^2}\frac{N^2}{f^2}\left[\frac{\tau}{\rho_0} + \alpha\frac{f}{N}E\right], \tag{42a}$$

$$\frac{\mathrm{d}E}{\mathrm{d}t} = -\alpha\frac{f}{N}ES - \lambda E, \tag{42b}$$

where $S = 2T/\left(LH^2\right)$ is the mean thermal windshear. Hence the time scale of the oscillatory response is set by two effects: the production of mean vertical shear due to the wind forced Eulerian overturning, and the efficiency of eddy energy generation for a given eddy energy and mean vertical shear,

$$\omega_0^2 = \underbrace{12\frac{1}{L^2}\frac{N^2}{f^2}\frac{\tau}{\rho_0}}_{\text{Mean shear production due to wind}} \times \underbrace{-\alpha\frac{f}{N}}_{\text{Energy conversion efficiency}}. \tag{43}$$

For the Southern Ocean relevant parameters listed in Table 1 the oscillatory time scale is $\tau_{\text{oscillation}} = 6.6$ years. Note that there is only a weak square root dependence on the key parameters, and hence a decadal oscillatory time scale is obtained for a broad range of plausible parameters; see Figure 3.

The oscillatory time scale (Equation 41) scales inversely with the square root of the wind stress forcing τ and also inversely with the square root of the efficiency parameter α, but is independent of the eddy energy dissipation rate λ. Changing the eddy energy dissipation rate changes the critical mean thermal windshear at which baroclinic

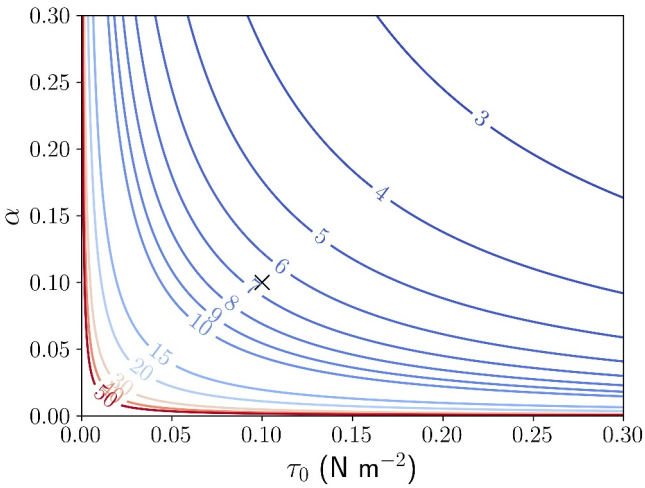

Figure 3. The oscillatory time scale, in years, given by Equation 41 for different values of τ and α. The black cross corresponds to $\tau = 0.1$ N m^{-2} and $\alpha = 0.1$. Other parameters are as in Table 1.

instability is sufficiently strong to overcome the linear energy dissipation—and hence sets the mean thermal wind transport at steady state—but the oscillatory time scale is set by the wind driven Eulerian mean overturning and the generation of eddy energy by baroclinic instability.

For $E_0 = 0$ the Hamiltonian structure allows the non-linear orbit time scale to be computed using action-angle coordinates, without linearizing. Time scales, for the Southern Ocean relevant parameters as in Table 1, are shown in Figure 1. These time scales are computed using fourth order finite differencing of the Hamiltonian contour areas, with the Hamiltonian contour areas computed using a method based on Simpson's rule. Even with very large perturbations away from the fixed point, associated with variations in mean thermal wind transport of order 100%, the time scale retains the same order of magnitude.

4.2. Oscillatory Forcing

Adding an oscillatory component to the wind stress

$$\tau \to \tau[1 + \epsilon \sin(\omega t)], \tag{44}$$

for some $\omega > 0$, if we consider the linearized system for the Hamiltonian case $E_0 = 0$, then the system reduces to a standard forced linear oscillator with a standard resonant response near the natural angular frequency ω_0, noting that here the logarithm of the non-dimensionalized eddy energy plays the role of the "displacement," and the non-dimensionalized transport perturbation the role of the "momentum."

As per the standard result for a damped linear oscillator, for high frequencies, $\omega > \omega_0$, in the linearized case with $E_0 = 0$ the mean thermal wind transport response lags the wind forcing by $\pi/2$, and the eddy energy response is out of phase with the wind forcing. For low frequencies, $\omega < \omega_0$, the mean thermal wind transport response leads the wind forcing by $\pi/2$, and the eddy energy response is in phase with the wind forcing. This appears to be a particularly accessible result which could be tested in more complicated models.

Numerical simulations of the non-linear Ambaum and Novak (2014) system with oscillatory forcing are described in Federer (2021).

4.3. Stochastic Forcing

The problem can be generalized to the case of stochastic forcing by instead considering

$$\tau \to \tau[1 + X_t], \tag{45}$$

where X_t is a stochastic process. Here stochastic processes depending on t or $\tilde{t}$ are denoted using subscripts.

If X_t is an Ornstein-Uhlenbeck process then in an appropriate short decorrelation time scale limit (see Pavliotis, 2014, Section 5.1) we now obtain the stochastic differential equations

$$\mathrm{d}T_t = 6\frac{H^2}{L}\frac{N^2}{f^2}\left[\frac{\tau}{\rho_0} + \alpha\frac{f}{N}E_t\right]\mathrm{d}t + 6\frac{H^2}{L}\frac{N^2}{f^2}\sqrt{\frac{2\mathbb{V}\left(\frac{\tau}{\rho_0}\right)}{\gamma}}\mathrm{d}W_t, \tag{46a}$$

$$\mathrm{d}E_t = \left[-2\alpha\frac{1}{LH^2}\frac{f}{N}T_t - \lambda\right]E_t\mathrm{d}t + \lambda E_0\mathrm{d}t, \tag{46b}$$

where $\mathbb{V}(\tau) = \rho_0^2\mathbb{V}\left(\tau/\rho_0\right)$ is the wind stress variance and $1/\gamma$ the wind stress decorrelation time scale.

For $E_0 = 0$ it follows, using Itô's formula, that

$$\frac{\mathrm{d}\mathbb{E}(\mathcal{H}_{\tilde{t}})}{\mathrm{d}\tilde{t}} = \frac{1}{2}\tilde{\sigma}^2. \tag{47}$$

where $\mathcal{H}$ is the Hamiltonian defined in (Equation 36), and where

$$\tilde{\sigma} = \frac{\rho_0}{\tau}\tilde{\omega}_0^2\sqrt{\lambda}\sqrt{\frac{2\mathbb{V}\left(\frac{\tau}{\rho_0}\right)}{\gamma}}. \tag{48}$$

Hence by perturbing the Hamiltonian system by adding stochastic wind forcing the system drifts in expectation toward higher Hamiltonian values, associated with longer period orbits, further from the fixed point.

For $E_0 \neq 0$ we instead obtain

$$\frac{\mathrm{d}\mathbb{E}(\mathcal{H}_{\tilde{t}})}{\mathrm{d}\tilde{t}} = \mathbb{E}\left[\tilde{\omega}_0^2\tilde{E}_0\left(1 - \frac{1}{\tilde{E}_{\tilde{t}}}\right)\right] + \frac{1}{2}\tilde{\sigma}^2. \tag{49}$$

At steady state a simple expression for the expectation of one over the eddy energy is obtained,

$$\mathbb{E}\left(\frac{1}{\tilde{E}_{\tilde{t}}}\right) = 1 + \frac{1}{2}\frac{1}{\tilde{\omega}_0^2}\frac{\tilde{\sigma}^2}{\tilde{E}_0}, \tag{50}$$

or, restoring dimensions,

$$\mathbb{E}\left(\frac{1}{E_t}\right) = -\alpha\frac{f}{N}\frac{\rho_0}{\tau}\left[1 + 12\frac{1}{L^2}\frac{N^2}{f^2}\frac{1}{\lambda}\frac{1}{E_0}\frac{\mathbb{V}\left(\frac{\tau}{\rho_0}\right)}{\gamma}\right]. \tag{51}$$

As the wind stress variance $\mathbb{V}(\tau)$ increases, the expectation of one over the eddy energy also increases. This counter-intuitive behavior is consistent with the dynamics being forced away from the fixed point, since orbits further from the fixed point spend relatively longer at lower eddy energy. The magnitude of the departure of the expectation from the steady state value is controlled by the competition between the magnitude of the stochastic forcing due to the wind stress, and the decay toward the steady state due to the background eddy energy term. The second term in Equation 50 expresses the non-dimensional relative strength of these two effects on the eddy energetics.

Figures 4–6 show the results from numerical solutions. The background eddy energy is set to a weak value of $E_0/E_* = 0.01$. The stochastic forcing is set via $\tilde{\sigma} = 0.04$, corresponding to a wind stress standard deviation of 128% of the mean wind stress for a wind stress decorrelation time scale of 1 week. Other parameters as in Table 1. The numerical calculations apply Strang splitting, with half Euler-Maruyama steps for the stochastic term before and after one full implicit mid-point rule step for the deterministic terms, and with a time step size of $10^{-3}\tau_{\text{oscillation}}$. The dynamics is perturbed away from the fixed point, although the effect on the characteristic oscillatory time scale is small—the mean Hamiltonian contour, averaged from $t > 95\tau_{\text{oscillation}}$ to $t \leq 100\tau_{\text{oscillation}}$ and over 10,000 independent realizations, is associated with an orbit time scale 4.6% larger than that at the fixed point. At these Southern Ocean relevant parameters, while the influence of the stochastic forcing on the mean thermal wind transport appears relatively more modest, the response of the eddy energy is substantial (noting that the *logarithm* of the non-dimensional eddy energy is shown). For the contour associated with the average of the Hamiltonian, the maximum mean thermal wind transport is 1.9 times the minimum, but the maximum eddy energy is 8.6 times the minimum. Hence this simple model suggests that a more substantial response to stochastic wind forcing may be seen through its effect on the ocean turbulence, rather than through the behavior of the mean. This effect arises not through direct driving of the turbulence, but instead through a perturbation of the system toward dynamics associated with larger excursions in eddy energy.

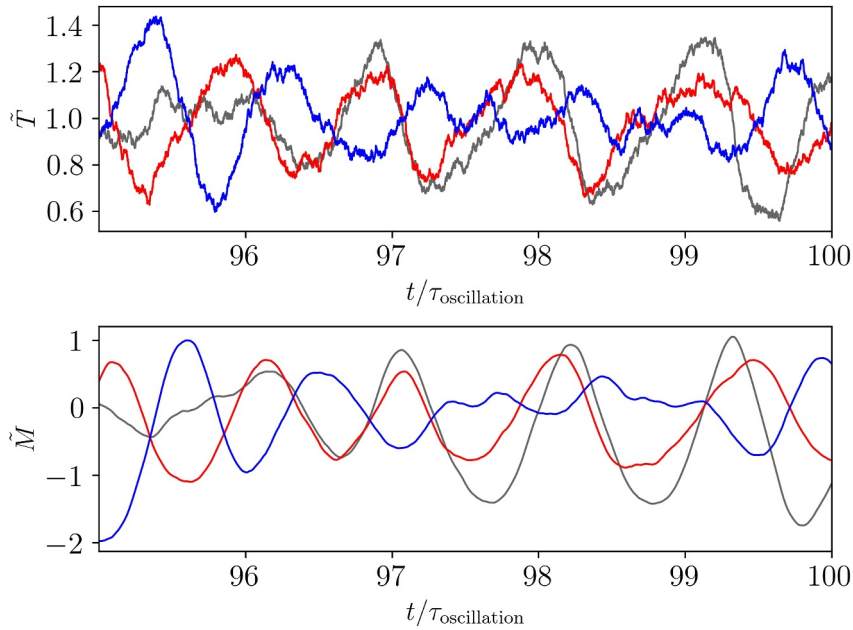

Figure 4. Time series for three independent realizations of the stochastically forced system (Equation 46), with $\tilde{\omega}_0^2 = 0.09$, $\tilde{E}_0 = 0.01$, and $\tilde{\sigma} = 0.04$.

5. Conclusions

This article describes an idealized two component dynamical system for Southern Ocean mean zonal thermal wind transport, coupled to a parameterized mesoscale eddy field. The model captures the evolution of a planetary geostrophic channel with a linear mean density profile and constant stratification. The GEOMETRIC form of the Gent–McWilliams parameterization is used, and combined with a model for a domain integrated eddy energy budget.

In the case of linear damping and zero eddy energy background term the system is Hamiltonian, and is (up to the definition of constants) equivalent to the non-linear oscillator of Ambaum and Novak (2014) and the system of Ong et al. (2024). The steady state mean thermal wind transport, set via the eddy energy balance, is insensitive to wind stress, capturing eddy saturation. The steady state eddy energy, set via the balance between Eulerian and eddy-induced overturning, or equivalently via a balance of vertical stress, scales with the eddy energy damping rate, capturing the principle of frictional control. The system oscillates at a characteristic oscillatory time scale, set by the combined effect of mean shear generation by the Eulerian overturning and the efficiency of eddy energy generation for a given mean vertical shear and eddy energy. For Southern Ocean relevant parameters the characteristic oscillatory time scale is decadal, with only a weak dependence on the parameter values. The introduction of stochastic wind forcing perturbs the system from equilibrium and leads to relatively large excursions in eddy energy.

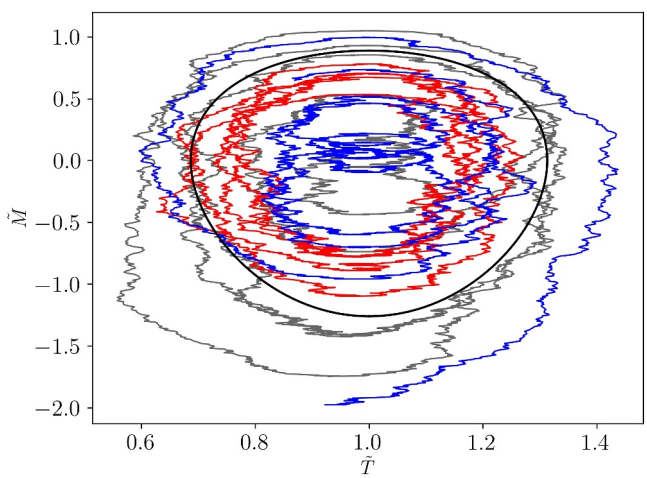

Figure 5. Phase portrait for the realizations shown in Figure 4. The black contour shows the Hamiltonian contour associated with the time average of the Hamiltonian from $t > 95\tau_{\text{oscillation}}$ to $t \leq 100\tau_{\text{oscillation}}$, averaged over 10,000 independent realizations (three of which are the realizations shown here).

There are a number of possible generalizations for the dynamical system. While we have assumed a fixed linear vertical stratification, a fixed but more general vertical stratification can be considered—see Appendix B. Since the equations are arrived at by imposing a specific one-dimensional basis for density perturbations, the system is naturally extended by increasing the size of this basis, for example, to permit time varying vertical stratification. The channel may then also be coupled to an inter-hemispheric basin, to yield a version of the Allison et al. (2011) model. We note the recent work of Kobras

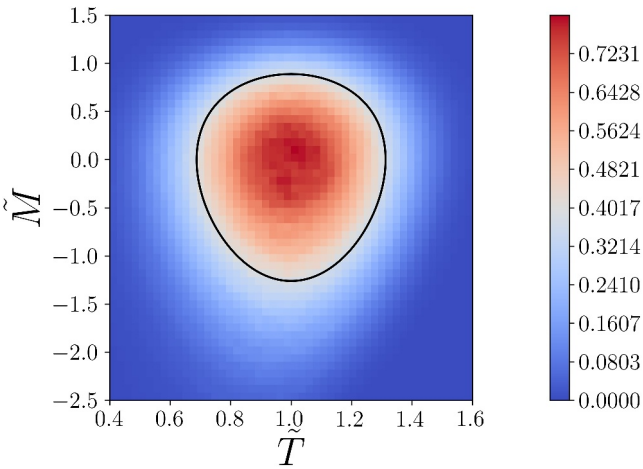

Figure 6. Two-dimensional normalized histogram for 10,000 independent realizations of the stochastically forced system (Equation 46), with $\tilde{\omega}_0^2 = 0.09$, $\tilde{E}_0 = 0.01$, and $\tilde{\sigma} = 0.04$. The values obtained after each time step of size $10^{-3}\tau_{\text{oscillation}}$, for $t > 95\tau_{\text{oscillation}}$ to $t \leq 100\tau_{\text{oscillation}}$ and for each realization, are binned using a 50×50 array. 0.89% of values are outside the considered range of $\tilde{T}$ and $\tilde{M}$. The black contour is associated with the average of the Hamiltonian, and is as in Figure 5.

et al. (2022, 2024) in the atmospheric context, which derive reduced order models for the two-level quasigeostrophic Phillips model on a β-plane, and obtain a six or eight dimensional dynamical system respectively. Although our model is simpler, complex models can display a richer structure, such as bifurcation of steady states (Kobras et al., 2022), and dependence on eddy geometry (Kobras et al., 2022, 2024). While an interesting avenue to pursue, an exploration into higher order models is beyond the scope of the present work, which was focused on minimal models for understanding eddy saturation and frictional control.

The idealized model considered here is also simplified by assuming that both the Eulerian and eddy-induced overturnings act on a thin layer at the domain boundaries. That is, both the Eulerian overturning stream function and eddy induced stream function are constant in the interior, and fall rapidly to zero near the boundaries. The steady state residual circulation is hence zero, and so this model cannot capture eddy compensation effects.

We note that the idealized model presented in this paper provides a dynamical explanation for the "eddy memory" mechanism explored in a series of papers by Manucharyan et al. (2017), Moon et al. (2021), Dijkstra et al. (2022), and Vanderborght et al. (2024). It would be of interest to explore the relation between these two approaches and, in particular, the relation and consistency of the oscillatory time scales predicted.

Marshall et al. (2017) outlined the key principles of eddy saturation and frictional control which are suggested under GEOMETRIC scalings, but considered only the equilibrium response. This article has considered a simple dynamical extension, so that key dynamical features can be identified. However it is clearly of interest to see if these features persist and can be observed in numerical models. This strongly motivates further study of the frequency response of less idealized Southern Ocean relevant models, for example, using an approach similar to that described in Sinha and Abernathey (2016), and which could be used to investigate and test dynamical predictions made under GEOMETRIC scalings.

The discussion of the oscillatory time scale is predicated on the assumption that the deviations from the Hamiltonian case are sufficiently weak. However an increased eddy energy background term, or increased influence of non-linear eddy energy damping, shortens the decay time scale. For the Southern Ocean relevant parameters in Table 1, with linear energy damping, the decay time scale equals the oscillatory time scale for $E_0/E_* = 9.4\%$, and the oscillatory behavior is lost entirely from the linearized dynamics at $E_0/E_* \geq 60\%$. In the stochastic case the numerical calculations made use of a weak eddy energy background combined with a strong stochastic wind forcing. Strengthening the eddy energy background term, or weakening the stochastic forcing, each weaken departures from the steady state. Combined, these effects may make observing an oscillatory time scale in a non-idealized setting challenging. However the simple model suggests that, with Southern Ocean relevant parameters, while variations in mean thermal wind transport may be more modest, the eddy energetics may be more sensitive to non-steady wind forcing, due to the potential for rapid growth in eddy energy.

Appendix A: Non-Linear Eddy Energy Dissipation

The parameterized eddy energy Equation 27 is modified to

$$\frac{\mathrm{d}E}{\mathrm{d}t} = \frac{1}{LH}\int_{-L/2}^{L/2}\int_{-H}^{0} \kappa_{\text{GM}}\left(\frac{\partial b}{\partial y}\right)^2\left(\frac{\partial b}{\partial z}\right)^{-1} \mathrm{d}z\,\mathrm{d}y - \lambda\left(\frac{E}{E_1}\right)^{a-1} E + \lambda E_0, \tag{A1}$$

for some dissipation exponent $a > 0$. Proceeding as before the dynamical system now becomes

$$\frac{\mathrm{d}T}{\mathrm{d}t} = 6\frac{H^2}{L}\frac{N^2}{f^2}\left[\frac{\tau}{\rho_0} + \alpha\frac{f}{N}E\right], \tag{A2}$$

$$\frac{\mathrm{d}E}{\mathrm{d}t} = \left[-2\alpha \frac{1}{LH^2}\frac{f}{N}T - \lambda\left(\frac{E}{E_1}\right)^{a-1}\right]E + \lambda E_0. \tag{A3}$$

The steady state eddy energy is unchanged. The steady state mean thermal wind transport becomes

$$T_* = -\frac{1}{2}\frac{1}{\alpha}LH^2\frac{N}{f}\lambda\left[\left(\frac{E_*}{E_1}\right)^{a-1} - \frac{E_0}{E_*}\right], \tag{A4}$$

and the linearized decay scale becomes

$$\tau_{\mathrm{decay}} = \frac{2}{\frac{E_0}{E_*} + (a-1)\left(\frac{E_*}{E_1}\right)^{a-1}}\frac{1}{\lambda}. \tag{A5}$$

Note that now, even for $E_0 = 0$, $a > 1$ leads to decay toward this fixed point. That is, $a > 1$ is an alternative mechanism for breaking the Hamiltonian structure.

Since the equilibrium eddy energy E_* scales linearly with the wind stress magnitude, for $E_0 > 0$ and $a = 1$ the decay time scale scales linearly with the wind stress magnitude, while for $E_0 = 0$ and $a > 1$ the decay time scale decreases with increasing wind stress magnitude.

The Ambaum and Novak (2014) model is now obtained as a special case for $a = 1$ and $\tilde{E}_0 = 0$. The case $p = 2$ and $\tilde{E}_0 = 0$ is considered in Federer (2021).

Appendix B: Generalized Vertical Stratification

The mean buoyancy profile in Equation 8 is generalized to (again defined up to a constant)

$$b(y,z,t) = m(t)y + N_0^2 R(z), \tag{B1}$$

where $R(z)$ is some function defined such that $R(-H) = -H$, $R(0) = 0$, and N_0 is a constant. We can no longer assume a z-independent Gent–McWilliams coefficient, and so instead use

$$\kappa_{\mathrm{GM}} = \alpha E S(z)\frac{N_0}{|m|} \tag{B2}$$

for non-negative $S(z)$ with maximum value one on $z \in [-H, 0]$.

Repeating the derivation, assuming spatially constant α (in the interior), the non-dimensional dynamical system (Equation 32) is arrived at as before, but with a modified non-dimensional mean thermal wind transport scale

$$\hat{T} = -\frac{1}{2}\frac{1}{\alpha}LH^2\frac{N_0}{f}\lambda\frac{H}{H_R}, \tag{B3}$$

non-dimensional energy scale

$$\hat{E} = -\frac{1}{\alpha}\frac{N_0}{f}\frac{\tau}{\rho_0}\frac{H}{H_S}, \tag{B4}$$

and non-dimensional squared angular frequency

$$\tilde{\omega}_0^2 = -12\alpha\frac{1}{L^2}\frac{N_0}{f}\frac{\tau}{\rho_0}\frac{1}{\lambda^2}\frac{H_R}{H}, \tag{B5}$$

with

$$H_S = \int_{-H}^{0} S(z)dz, \tag{B6a}$$

$$H_R = \int_{-H}^{0} S(z)\left(\frac{dR}{dz}\right)^{-1} dz. \tag{B6b}$$

Data Availability Statement

Scripts used to generate the figures in this article can be found in Maddison (2024).

Acknowledgments
JRM, DPM, and JM were supported by the Natural Environment Research Council [NE/R000999/1]. JM also acknowledges financial support from Hong Kong Research Grants Council via Grant 11308021. KM acknowledges the generous support of a David Richards Scholarship at Wadham College, Oxford. JRM acknowledges helpful discussions with Kostas Zygalakis and Jacques Vanneste. The authors thank the editor Stephen Griffies and the three anonymous reviewers for their helpful comments. This work was supported by the Natural Environment Research Council [NE/R000999/1]. This research was funded in whole, or in part, by the Natural Environment Research Council [NE/R000999/1]. For the purpose of open access, the author has applied a creative commons attribution (CC BY) license to any author accepted manuscript version arising.

References

Allison, L. C., Johnson, H. L., & Marshall, D. P. (2011). Spin-up and adjustment of the Antarctic Circumpolar Current and global pycnocline. *Journal of Marine Research*, *69*(2–3), 167–189. https://doi.org/10.1357/002224011798765330

Ambaum, M. H. P., & Novak, L. (2014). A nonlinear oscillator describing storm track variability. *Quarterly Journal of the Royal Meteorological Society*, *140*(685), 2680–2684. https://doi.org/10.1002/qj.2352

Bachman, S. D. (2019). The GM+E closure: A framework for coupling backscatter with the Gent and McWilliams parameterization. *Ocean Modelling*, *136*, 85–106. https://doi.org/10.1016/j.ocemod.2019.02.006

Bagaeva, E., Daninov, S., Oliver, M., & Juricke, S. (2020). Advancing eddy parameterizations: Dynamic energy backscatter and the role of subgrid energy advection and stochastic forcing. *Journal of Advances in Modeling Earth Systems*, *16*(4), e2023MS003972. https://doi.org/10.1029/2023MS003972

Bishop, S. P., Gent, P. R., Bryan, F. O., Thompson, A. F., Long, M. C., & Abernathey, R. P. (2016). Southern Ocean overturning compensation in an eddy-resolving climate simulation. *Journal of Physical Oceanography*, *46*(5), 1575–1592. https://doi.org/10.1175/JPO-D-15-0177.1

Cessi, P. (2008). An energy-constrained parameterization of eddy buoyancy flux. *Journal of Physical Oceanography*, *38*(8), 1807–1819. https://doi.org/10.1175/2007JPO3812.1

Dijkstra, H. A., Manucharyan, G., & Moon, W. (2022). Eddy memory in weakly-nonlinear two-layer quasi-geostrophic ocean flows. *The European Physical Journal Plus*, *137*(10), 1162. https://doi.org/10.1140/epjp/s13360-022-03360-9

Eden, C., & Greatbatch, R. J. (2008). Towards a mesoscale eddy closure. *Ocean Modelling*, *20*(3), 223–239. https://doi.org/10.1016/j.ocemod.2007.09.002

Farneti, R., Downes, S. M., Griffies, S. M., Marsland, S. J., Behrens, E., Bentsen, M., et al. (2015). An assessment of Antarctic Circumpolar Current and Southern Ocean meridional overturning circulation during 1958-2007 in a suite of interannual CORE-II simulations. *Ocean Modelling*, *94*, 84–120. https://doi.org/10.1016/j.ocemod.2015.07.009

Federer, M. P. (2021). *Predator-prey behaviour of storm tracks* [Master thesis]. ETH Zurich. https://doi.org/10.3929/ethz-b-000690363

Gent, P. R., & McWilliams, J. C. (1990). Isopycnal mixing in ocean circulation models. *Journal of Physical Oceanography*, *20*(1), 150–155. https://doi.org/10.1175/1520-0485(1990)020<0150:IMIOCM>2.0.CO;2

Gent, P. R., Willebrand, J., McDougall, T. J., & McWilliams, J. C. (1995). Parameterizing eddy-induced tracer transports in ocean circulation models. *Journal of Physical Oceanography*, *25*(4), 463–474. https://doi.org/10.1175/1520-0485(1995)025<0463:PEITTI>2.0.CO;2

Gnanadesikan, A. (1999). A simple predictive model for the structure of the oceanic pycnocline. *Science*, *283*(5410), 2077–2079. https://doi.org/10.1126/science.283.5410.2077

Hewitt, H. T., Roberts, M., Mathiot, P., Biastoch, A., Blockley, E., Chassignet, E. P., et al. (2020). Resolving and parameterising the ocean mesoscale in Earth system models. *Current Climate Change Reports*, *6*(4), 137–152. https://doi.org/10.1007/s40641-020-00164-w

Hughes, C. W., Meredith, M. P., & Heywood, K. J. (1999). Wind-driven transport fluctuations through Drake Passage: A southern mode. *Journal of Physical Oceanography*, *29*, 1971–1992. https://doi.org/10.1175/1520-0485(1999)029<1971:WDTFTD>2.0.CO;2

Jansen, M. F., Adcroft, A., Khani, S., & Kong, H. (2019). Toward an energetically consistent, resolution aware parameterization of ocean mesoscale eddies. *Journal of Advances in Modeling Earth Systems*, *1*(8), 1–17. https://doi.org/10.1029/2019MS001750

Jansen, M. F., & Held, I. M. (2014). Parameterizing subgrid-scale eddy effects using energetically consistent backscatter. *Ocean Modelling*, *80*, 36–48. https://doi.org/10.1016/j.ocemod.2014.06.002

Kobras, M., Ambaum, M. H. P., & Lucarini, V. (2022). Eddy saturation in a reduced two-level model of the atmosphere. *Geophysical & Astrophysical Fluid Dynamics*, *116*(1), 38–55. https://doi.org/10.1080/03091929.2021.1990912

Kobras, M., Lucarini, V., & Ambaum, M. H. P. (2024). Latitudinal storm track shift in a reduced two-level model of the atmosphere. *Physica D: Nonlinear Phenomena*, *458*, 133926. https://doi.org/10.1016/j.physd.2023.133926

Lorenz, E. N. (1984). Irregularity: A fundamental property of the atmosphere. *Tellus A*, *36A*(2), 98–110. https://doi.org/10.1111/j.1600-0870.1984.tb00230.x

Maddison, J. R. (2024). Scripts for 'A two-dimensional model for eddy saturation and frictional control in the Southern Ocean' [Software]. *Zenodo*. https://doi.org/10.5281/zenodo.14514833

Mak, J., Avdis, A., David, T. W., Lee, H. S., Na, Y., & Yan, F. E. (2022). On constraining the mesoscale eddy energy dissipation time-scale. *Journal of Advances in Modeling Earth Systems*, *14*(11), e2022MS003223. https://doi.org/10.1029/2022MS003223

Mak, J., Maddison, J. R., Marshall, D. P., & Munday, D. R. (2018). Implementation of a geometrically informed and energetically constrained mesoscale eddy parameterization in an ocean circulation model. *Journal of Physical Oceanography*, *48*(10), 2363–2382. https://doi.org/10.1175/JPO-D-18-0017.1

Mak, J., Marshall, D. P., Maddison, J. R., & Bachman, S. D. (2017). Emergent eddy saturation from an energy constrained eddy parameterisation. *Ocean Modelling*, *112*, 125–138. https://doi.org/10.1016/j.ocemod.2017.02.007

Mak, J., Marshall, D. P., Madec, G., & Maddison, J. R. (2022). Acute sensitivity of global ocean circulation and heat content to eddy energy dissipation time-scale. *Geophysical Research Letters*, *49*(8), e2021GL097259. https://doi.org/10.1029/2021GL097259

Manucharyan, G. E., Thompson, A. F., & Spall, M. A. (2017). Eddy memory mode of multidecadal variability in residual-mean ocean circulations with application to the beaufort gyre. *Journal of Physical Oceanography*, *47*(4), 855–866. https://doi.org/10.1175/jpo-d-16-0194.1

Marshall, D. P., Ambaum, M. H. P., Maddison, J. R., Munday, D. R., & Novak, L. (2017). Eddy saturation and frictional control of the Antarctic Circumpolar Current. *Geophysical Research Letters*, *44*(1), 286–292. https://doi.org/10.1002/2016GL071702

Marshall, D. P., Maddison, J. R., & Berloff, P. S. (2012). A framework for parameterizing eddy potential vorticity fluxes. *Journal of Physical Oceanography*, *42*(4), 539–557. https://doi.org/10.1175/JPO-D-11-048.1

Moon, W., Manucharyan, G. E., & Dijkstra, H. A. (2021). Eddy memory as an explanation of intraseasonal periodic behaviour in baroclinic eddies. *Quarterly Journal of the Royal Meteorological Society*, *147*(737), 2395–2408. https://doi.org/10.1002/qj.4030

Munday, D. R., Johnson, H. L., & Marshall, D. P. (2013). Eddy saturation of equilibrated circumpolar currents. *Journal of Physical Oceanography*, *43*(3), 507–532. https://doi.org/10.1175/JPO-D-12-095.1

Novak, L., Ambaum, M. H. P., & Harvey, B. J. (2018). Baroclinic adjustment and dissipative control of storm tracks. *Journal of the Atmospheric Sciences*, *75*(9), 2955–2970. https://doi.org/10.1175/JAS-D-17-0210.1

Novak, L., Ambaum, M. H. P., & Tailleux, R. (2017). Marginal stability and predator–prey behaviour within storm tracks. *Quarterly Journal of the Royal Meteorological Society*, *143*(704), 1421–1433. https://doi.org/10.1002/qj.3014

Olbers, D., & Lettmann, K. (2007). Barotropic and baroclinic processes in the transport variability of the Antarctic Circumpolar Current. *Ocean Dynamics*, *57*(6), 559–578. https://doi.org/10.1007/s10236-007-0126-1

Ong, E. Q. Y., Doddridge, E., Constantinou, N. C., Hogg, A. M., & England, M. H. (2024). Intrinsically episodic Antarctic shelf intrusions of Circumpolar Deep Water via canyons. *Journal of Physical Oceanography*, *54*(5), 1195–1210. https://doi.org/10.1175/JPO-D-23-0067.1

Pavliotis, G. A. (2014). *Stochastic processes and applications*. Springer Science+Business Media.

Pedlosky, J. (1970). Finite-amplitude baroclinic waves. *Journal of the Atmospheric Sciences*, *27*(1), 15–30. https://doi.org/10.1175/1520-0469(1970)027<0015:FABW>2.0.CO;2

Sinha, A., & Abernathey, R. P. (2016). Time scales of Southern Ocean eddy equilibration. *Journal of Physical Oceanography*, *46*(9), 2785–2805. https://doi.org/10.1175/JPO-D-16-0041.1

Straub, D. N. (1993). On the transport and angular momentum balance of channel models of the Antarctic Circumpolar Current. *Journal of Physical Oceanography*, *23*(4), 776–782. https://doi.org/10.1175/1520-0485(1993)023<0776:OTTAAM>2.0.CO;2

Sura, P., & Gille, S. T. (2003). Interpreting wind-driven Southern Ocean variability in a stochastic framework. *Journal of Marine Research*, *61*(3), 313–334. https://doi.org/10.1357/002224003322201214

Thompson, A. F., Stewart, A. L., & Bischoff, T. (2016). A multibasin residual-mean model for the global overturning circulation. *Journal of Physical Oceanography*, *46*(9), 2583–2604. https://doi.org/10.1175/JPO-D-15-0204.1

Thompson, P. D. (1987). Large-scale dynamical response to differential heating: Statistical equilibrium states and amplitude vacillation. *Journal of the Atmospheric Sciences*, *44*(8), 1237–1248. https://doi.org/10.1175/1520-0469(1987)044<1237:LSDRTD>2.0.CO;2

Vanderborght, E., Demaeyer, J., Manucharyan, G., Moon, W., & Dijkstra, H. A. (2024). Physics of the eddy memory kernel of a baroclinic midlatitude atmosphere. *Journal of the Atmospheric Sciences*, *81*(3), 691–711. https://doi.org/10.1175/jas-d-23-0146.1

Yankovsky, E., Bachman, S. D., Smith, K. S., & Zanna, L. (2024). Vertical structure and energetic constraints for a backscatter parameterization of ocean mesoscale eddies. *Journal of Advances in Modeling Earth Systems*, *16*(7), e2023MS004093. https://doi.org/10.1029/2023MS004093